# THE OPTICS OF THE COMPRESSIBLE N = 2 VORTEX

Georgios H. Vatistas
Department of Mechanical and Industrial Engineering
Concordia University
Montreal Canada, H3G 1M8
vatistas@me.concordia.ca

Received July 2005, Accepted November 2005
No. 05-CSME-46, E.I.C. Accession 2898

## ABSTRACT

This paper deals with the refracted shadows generated by the $n = 2$ compressible vortex. A more pragmatic picture of the optical phenomenon emerges when the flow instead of being isentropic is permitted to transfer heat and dissipate mechanical energy. The visual side of the formulation adheres to the long-established shadowgraph technique. It is shown that although the constant entropy hypothesis retains the qualitative nature of the phenomenon, the present approach improves on the quantitative side of the problem. It reveals that the central dark disk boundary does not mark the vortex core radius, renders the center of the vortex slightly darker, and the halo considerably brighter than the earlier isentropic flow estimates. Furthermore, it offers an alternative explanation for the peculiar set of alternating dark and bright circular bands that appeared in the shadow imprints of an earlier blade tip vortex experiment. The improved methodology can now be used to advance the experimental description of compressible vortices through shadowgraphy.

# L' OPTIQUE DU MODELE DE TOURBILLONS COMPRESSIBLE N = 2

## RESUME

Ce papier concerne l'ombre reflétée par le model de tourbillon compressible $n = 2$. Une image plus réaliste du phénomène optique émerge lorsque la dissipation et conduction de chaleur sont permises. Le coté optique de l'étude correspond aux techniques bien connues de shadowgraph. Il est monter que bien que l'hypothèse d'entropie constante retienne qualitativement la nature du phénomène ; cette présente approche améliore les aspects quantitatifs. La présente approche montre clairement que la limite du disque noir ne marque pas le rayon du cœur du tourbillon ; elle rend que le centre du tourbillon plus noir et l'extérieur plus clair. De plus cette approche explique le phénomène d'apparition de couronnes alternativement sombre et clair observées sur le shadowgraph des tourbillons aux extrémités des pales d'un hélicoptère. Cette méthode peut être utilisé pour améliorer la description des tourbillon compressible à travers l'utilisation du shadowgraph.

## Nomenclature

| | |
|---|---|
| $C$ | constant $(m^3/kg)$ |
| $c_o$, $c_1$ | dimensionless general constants |
| $c_p$, $c_v$ | heat capacities constant pressure and volume respectively $(W\,s/kg\,K)$ |
| $E$ | light intensity $(Lm/m^2)$ |
| $H$ | normalized axial velocity component $(\beta\,Re\,h)$ |
| $k$ | thermal conductivity $(W/m\,K)$ |
| $L$ | large dimensionless number |
| $l$ | distance from the test section to the image plane $(m)$ |
| $M_o$ | vortex Mach number $(V_{\theta c}/\sqrt{\gamma R\,T_\infty})$ |
| $n$ | vortex exponent of the $n$ – family |
| $O$ | order of magnitude |
| $p$ | static pressure $(Pa)$ |
| $Pr$ | Prandtl number $(\mu c_p/k)$ |
| $q$ | total velocity vector $(m/s)$ |
| $R$ | gas constant $(J/kg\,K)$ |
| $Re$ | vortex Reynolds number $(\rho_\infty V_{\theta c}\,r_c/\mu)$ |
| $r$, $\theta$, $z$ | radial, azimuthal, and axial coordinates $(m)$ |
| $r_c$ | core radius $(m)$ |
| $r_d$ | central dark disk radius $(m)$ |
| $T$ | static temperature $(K)$ |
| $t$ | dimensionless dummy variable |
| $U$ | normalized radial velocity component $(\beta\,Re\,u)$ |
| $u$ | dimensionless radial velocity component $(V_r/V_{\theta c})$ |
| $V$ | normalized tangential velocity component |
| $V_r$, $V_\theta$, $V_z$ | radial, tangential and axial velocity components $(m/s)$ |
| $V_{\theta c}$ | core tangential velocity $(\Gamma_\infty/2\pi r_c,\ m/s)$ |
| $v$ | dimensionless tangential velocity component $(V_\theta/V_{\theta c})$ |
| $w$ | dimensionless axial velocity component $(V_z/V_{\theta c} = z\,h)$ |
| $x$, $y$ | Cartesian coordinates $(m)$ |
| *Greek characters* | |
| $\alpha$ | angle of refraction |
| $\beta$ | dimensionless density $(\rho/\rho_\infty)$ |
| $\Gamma_\infty$ | vortex circulation $(m^2/s)$ |
| $\gamma$ | specific heat ratio $(c_p/c_v)$ |
| $\delta$ | dimensionless small number |
| $\delta\alpha$ | finite change of the angle of refraction |
| $\delta y$ | finite change in the y – direction $(m)$ |
| $\eta$ | refraction index |
| $\Theta$ | dimensionless static temperature $(T/T_\infty)$ |
| $\vartheta$ | dimensionless dummy variable |
| $\kappa$ | vortex strength $(\Gamma_\infty/2\pi,\ m^2/s)$ |
| $\lambda$ | dimensionless distance from the test section to the image plane $(l/r_c)$ |

| | |
|---|---|
| $\mu$ | fluid viscosity $(kg/m\,s)$ |
| $\xi, \zeta$ | dimensionless coordinates $(r/r_c \text{ and } z/r_c)$ |
| $\Pi$ | dimensionless static pressure $(p/\rho_\infty V_{\theta c}^2)$ |
| $\rho$ | fluid density $(kg/m^3)$ |
| $\Sigma$ | dimensionless light intensity |
| $\sigma$ | lumped parameter $(\rho_\infty C)$ |
| $\Phi$ | viscous dissipation function $(W/m^3)$ |
| *subscripts* | |
| *im pl* | image plane |
| $\infty$ | properties far away the vortex center |
| *1, 2* | optical stations 1 and 2 |
| *c* | vortex core |
| *d* | dark disk boundary |

## 1. Introduction

One way to resolve experimentally a compressible vortex, in a non-intrusive way, is through the method of shadow. This well-known fundamental technique[1] takes advantage of the fact that the value of the refraction index depends on the density of the transparent medium. Light rays emerging from a test section, where the density of the gas varies, refract thus casting a corresponding shadow on the image plane. In reverse, the density variation can be experimentally determined from the shadow light intensity signature. The rest of the fluid properties can then be recovered via a suitable vortex model.

The early beginnings of a systematic research on the optical properties of Rankine-like vortices are traced back to the contribution of Berry and Hajanal[2]. In addition to the visual effects produced by floating objects in liquids, they also dealt with those of dissipating eddies approached from the principle of caustics. The investigations of Sterling et al.[3] were exclusively preoccupied with the cause that had as an effect the emergence of a centrally located dark disk surrounded by a halo (corona) on the image plane when liquid vortices were uniformly illuminated from above. The subdued interest in this topic has been driven by curiosity alone since there was no apparent immediate practical application of the phenomenon.

Two systems that may not necessarily resemble each other physically are considered analogous if both are described by a corresponding set of equations. A well-known paradigm of such systems is the shallow water hydraulic analog to the 2-D compressible gaseous flow[4]. This renowned likeness between the two problems suggests that the free surface profile in hydraulics corresponds to the density variation in gas dynamics. Although the topology for this homology is not complete, the main physical manifestations come into view even though the liquid may not be shallow, the field isentropic, or moreover the specific heat ratio of the gas equal to two. The refraction angle depends on the free surface rise and the gas density variation in liquid and compressible vortices respectively. Since the radial profiles of liquid elevation and density are similar, when illuminated, they must project analogous refracted patterns on the image plane. It is therefore not surprising to also find comparable to the liquid free surface refracted light patterns of Sterling et al.[3] in the visualization experiments of compressible helicopter rotor tip vortices by Parthasarthy et al.[5], Swanson and Light[6], and Bagai and Leishman[7].

Furthermore, since the last is a fundamental property of compressible fluid flows it must have appeared in past shadowgraph experiments that dealt with compressible flows containing vortices. The latter is present in a diffraction image produced by a shock wave/wedge interaction found in the album of fluid motion by Van Dyke[8] (Fig. 241, p. 147), where the dark-disk/corona property of the compressible vortices is amply evident.

The visualization of compressible vortices through the method of shadow has received considerable attention from the helicopter community[5-7,9]. Heavily laden helicopter blades may emit tip vortices that are in the compressible region of the flow spectrum. Upon illumination, density changes trigger a variation in the refraction index thus making the vortex visible.

The goal of Parthasarthy et al.[5] and Norman and Light[9] investigations, was to develop an experimental technique, based on the fundamental principles of shadowgraphy, in order to estimate several flow properties of helicopter tip vortices.

Swanson and Light[6] presented shadowgraph flow visualizations produced by a tilt rotor wing in hover revealing the emergence of some unusual banded shadow patterns. The nature of these peculiar shade manifestations will be discussed in the last section of this paper. The earlier theoretical treatment by Parthasarthy et al.[5] Norman and Light[9] were based on simple gas dynamics and optical principles complimented by several empirical formulae. Bagai and Leishman[7] outlined the potential practical importance of such a non-intrusive diagnostic technique, and contributed a methodical analytical treatment of the problem, assuming the flowfield to be homentropic. They then proceeded to demonstrate that this method could indeed offer an effective way to measure several of the vortex flow properties non-intrusively, where separation (due to centrifugal action) of seed particles near the axis of rotation associated with the traditional optical methods such as Laser Doppler Anemometry (LDA) and Particle Image Velocimetry (PIV), is absent.

An improved account for the optics will require a better compressible flow description. The constant entropy hypothesis prevents the flow from being general, i.e. irreversible and diabatic. Here we employ the recently derived extension of the incompressible $n = 2$ vortex[10] which accounts for density variation[11] without invoking homentropy. The optical analysis follows the traditional shadowgraph method found in the technical literature[1,12] assuming a polar geometry. The cause of the evolved refraction pattern on the image plane is shown to be a direct consequence of the deflection of the emerging rays, which is proportional to the density gradient of the gas within the test section.

## 2. Formulation of the problem

The gas dynamic side of the problem follows closely the analysis described in Ref. 11. Since this aspect of the phenomenon is very pertinent to our subsequent optical development it will be described here in detail.

Consider the motion of a steady, compressible, axisymmetric vortex. We are interested in solutions of a particular category of vortices[10,13] in which the velocity in this case is of the general form:

$$\boldsymbol{q}\ [\ V_r(r\ ),\ V_\theta(r\ ),\ V_z = z\,fn\ (r)]$$

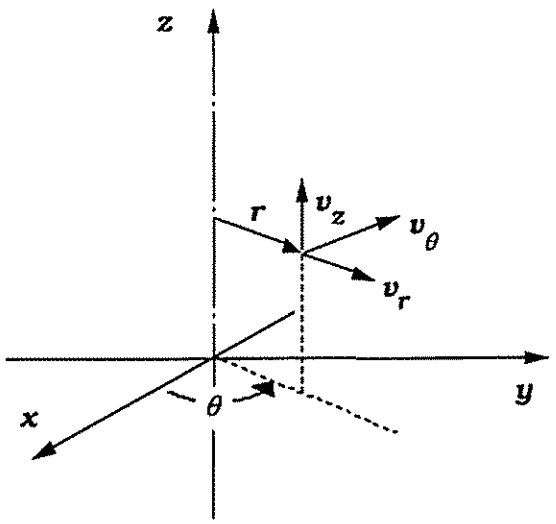


Figure 1. The coordinate system

All variables are defined in the *nomenclature* and the coordinate system used is illustrated in Fig. 1.

Starting point of the theory are the simplified equations of continuity, Navier-Stokes, energy, and the equation of state of a calorically perfect gas:

*Conservation of mass*

$$\frac{1}{\xi}\frac{\partial \beta u \xi}{\partial \xi} + \beta h = 0 \qquad (1)$$

$1\delta \qquad 1\delta$

*radial momentum*

$$Re\ \beta\left\{\ u\ \frac{\partial u}{\partial \xi}+h\ \frac{\partial u}{\partial \zeta}-\frac{v^2}{\xi}\ \right\}=-\ Re\frac{\partial \Pi}{\partial \xi}+\frac{\partial}{\partial \xi}\left\{\frac{1}{\xi}\frac{\partial u\ \xi}{\partial \xi}\right\}+\frac{\partial^2 u}{\partial \zeta^2} \qquad (2)$$

$1/\delta\ \ 1\quad \delta\ \ \delta\quad \delta\ \ \delta\quad 1\qquad 1/\delta\qquad\qquad \delta\qquad \delta$

*tangential momentum*

$$Re\ \ \frac{\beta u}{\xi}\frac{\partial V\xi}{\partial \xi}=\ \frac{\partial}{\partial \xi}\left\{\frac{1}{\xi}\frac{\partial V\ \xi}{\partial \xi}\right\} \qquad (3)$$

$1/\delta\ \ 1\ \delta\quad 1\qquad\qquad 1$

*axial momentum*

$$Re\,\beta\left\{\ u\ \frac{\partial h}{\partial \xi}\ +\ h^2\ \right\}=-\ \frac{Re}{\zeta}\ \frac{\partial \Pi}{\partial \zeta}+\frac{1}{\xi}\frac{\partial}{\partial \xi}\left\{\xi\frac{\partial h}{\partial \xi}\ \right\} \qquad (4)$$

$1/\delta\ 1\quad \delta\ \ \delta\quad \delta^2\qquad 1/\delta\qquad\qquad \delta$

*energy*

$$\frac{1}{\xi}\frac{\partial}{\partial \xi}\left\{\xi\frac{\partial \Theta}{\partial \xi}\right\}+\frac{\partial^2\ \Theta}{\partial \zeta^2}\ +Pr\,(\,\gamma-1\,)\,M_o^2 f=\beta\,Pr\,Re\left\{\ u\frac{\partial \Theta}{\partial \xi}+w\frac{\partial \Theta}{\partial \zeta}\right\}$$

$1\qquad 1\qquad\quad 1\quad\ 1\quad\ 1\ \ 1\quad\ 1\ \ 1\ 1/\delta\quad \delta\ 1\quad\ \delta\ \ 1$

$$-Pr\,Re\,(\,\gamma-1\,)\,M_o^2\left\{\ u\frac{\partial \Pi}{\partial \xi}+w\frac{\partial \Pi}{\partial \zeta}\right\} \qquad (5)$$

$1\ 1/\delta\quad 1\quad\ 1\qquad \delta\qquad\ \delta$

Where

$$f=2\left\{\left[\frac{\partial u}{\partial \xi}\right]^2+\left[\frac{u}{\xi}\right]^2+\ h\ ^2+\frac{1}{2}\left[\ \frac{\partial V}{\partial \xi}\ -\ \frac{V}{\xi}\right]^2\right.$$

$\delta\qquad \delta\qquad \delta^2\qquad\qquad 1\qquad 1$

$$\left.+\frac{1}{2}\left[\ \frac{\partial u}{\partial \zeta}+\zeta\frac{\partial h}{\partial \xi}\right]^2-\frac{1}{3}\left(\ \frac{\partial u}{\partial \xi}+\ \frac{u}{\xi}+h\right)^2+\frac{1}{3}\left[\frac{1}{\xi}\frac{d\,\beta u\ \xi}{d\xi}+\beta h\ \right]^2\right\}$$

$\delta\qquad \delta\qquad\qquad \delta\quad\ \delta\quad \delta\qquad\qquad\qquad 1\ \delta\quad\ 1\ \delta$

*equation of state*

$$\Pi = \frac{\beta\ \Theta}{\gamma\ M_o^2} \tag{6}$$

*1 1*

Subscript $c$ denotes values of the parameters at the core (defined as the radius where the tangential velocity attains its maximum).

Because we are dealing with strong vortices, the traditional assumption requiring that $u$ and $h << V$, is implemented. In terms of order of magnitude, if $V$ is of O (1), then $u$ and $h$ are small say of O ($\delta$), where $\delta \sim 1/Re$ (for example in aerodynamically produced vortices $Re \sim 10^5$) then one can bring the above system of equations into a simpler form. Note that this assumption is implicit in the theory that has produced all the previous classical vortex models such as for example Burgers[14] and Sullivan[15]. All the terms in Eqs. (1) and (3) are of the same order of magnitude and therefore both stay as they are.

Neglecting the terms in Eq. (2) of order $\delta$ we obtain,

$$\frac{\beta V^2}{\xi} = \frac{\partial \Pi}{\partial \xi} \tag{7}$$

The axial momentum Eq. (4) suggests that the static pressure should not vary appreciably in the $\zeta$-direction:

$$Re\frac{\partial \Pi}{\partial \zeta} \sim \delta, \quad or \quad \frac{\partial \Pi}{\partial \zeta} \sim \delta^2 \ \rightarrow \ \frac{\partial \Pi}{\partial \zeta} \approx 0$$

This points out that the pressure should be a sole function of $\xi$. The density, from the $\xi$-momentum, and the temperature, from the equation of state, must also depend on $\xi$ alone.

Therefore the energy equation simplifies into:

$$\frac{1}{\xi}\frac{d}{d\xi}\left(\xi\frac{d\ \Theta}{d\xi}\right) + Pr(\gamma - 1)M_o^2 f = \beta Pr\, Re\, u\frac{d\ \Theta}{d\xi} - Pr\, Re(\gamma - 1)M_o^2 u\frac{d\ \Pi}{d\xi} \tag{8}$$

Where

$$f = \xi^2 \left\{ \frac{d}{d\xi} \left[ \frac{V}{\xi} \right] \right\}^2$$

Letting $U = \beta\, Re\, u$ and $H = \beta\, Re\, h$, and replacing the pressure gradient by its equivalent $\beta V^2/\xi$, the governing equations transform into:

*continuity*

$$\frac{1}{\xi} \frac{d\, U\, \xi}{d\xi} + H = 0 \tag{9}$$

*radial momentum*

$$\frac{\beta V^2}{\xi} = \frac{d\Pi}{d\xi} \tag{10}$$

*tangential momentum*

$$\frac{U}{\xi} \frac{dV\, \xi}{d\xi} = \frac{d}{d\xi} \left\{ \frac{1}{\xi} \frac{d\, V\, \xi}{d\xi} \right\} \tag{11}$$

*energy*

$$\frac{1}{\xi} \frac{d}{d\xi} \left( \xi \frac{d\, \Theta}{d\xi} \right) + Pr\, U\, \frac{d\, \Theta}{d\xi} = -Pr\, (\gamma - 1)\, M_o^2 \left\{ U \frac{V^2}{\xi} + \xi^2 \left\{ \frac{d}{d\xi} \left[ \frac{V}{\xi} \right] \right\}^2 \right\} \tag{12}$$

*equation of state*

$$\Pi = \frac{\beta\, \Theta}{\gamma\, M_o^2} \tag{13}$$

The required boundary conditions are:

i. $\xi = 0,\ V(\xi) = U(\xi) = 0,\ and\ dH(\xi)/d\xi = d\Theta(\xi)/d\xi = 0$

ii. $\xi \to \infty,\ V(\xi)\,\xi, \Theta(\xi), \gamma M_o\, \Pi and\ \beta(\xi) \to 1$

The hydrodynamic portion consisting from Eqs. (9) and (11), has now exactly the same form as its incompressible counterpart[10,13]. By analogy, one of the known solutions for the velocity is:

$$U = -\frac{6\,\xi^3}{1+\xi^4} \tag{14}$$

$$H = \frac{24\,\xi^2}{\left(1+\xi^4\right)^2} \tag{15}$$

$$V = \frac{\xi}{\left(1+\xi^4\right)^{1/2}} \tag{16}$$

All the above velocity components reduce asymptotically to zero as $\xi \to \infty$. Because the actual radial and axial velocities involve the density,

$$u = -\frac{6\,\xi^3}{Re\,\beta\left(1+\xi^4\right)} \quad \text{and} \quad w/\zeta = \frac{24\,\xi^2}{Re\,\beta\left(1+\xi^4\right)^2} \tag{17}$$

both will be affected by compressibility. The meridional flow (in the $\xi$-$\zeta$ plane) velocity components keep the shapes of the incompressible vortex but increase in magnitude. On the other hand the tangential will not be affected by $\beta$. The last deduction is reasonably supported by past experiments[16-18].

Integrating the energy equation (12) and applying the temperature derivative boundary condition at $\xi = 0$ gives:

$$\Theta(\xi) = (\gamma - 1)\, Pr\, M_o^2 \int_0^{\xi} \frac{1}{\vartheta\left(1+\vartheta^4\right)^{3/2\ Pr}} \left\{ \int_0^{\vartheta} \frac{6t^5 + 2t^9}{\left(1+t^4\right)^{3-3/2\ Pr}}\, dt \right\} d\vartheta + c_o \tag{18}$$

The second boundary condition $\xi \to \infty$ yields,

$$c_o = 1 - (\gamma - 1)\, Pr\, M_o^2 \lim_{L\to\infty} \int_0^{L} \frac{1}{\vartheta\left(1+\vartheta^4\right)^{3/2\ Pr}} \left\{ \int_0^{\vartheta} \frac{6t^5 + 2t^9}{\left(1+t^4\right)^{3-3/2\ Pr}}\, dt \right\} d\vartheta$$

For the specific case where $Pr = 2/3$, integrating once the energy equation and application of the temperature boundary condition; for $\xi = 0$ gives:

$$\frac{d\Theta}{d\xi} = \frac{2}{3}(\gamma - 1)\, M_o^2 \frac{\xi^5}{\left(1+\xi^4\right)^2}$$

A second integration along with the condition at $\xi \to \infty$ provides the exact solution for the temperature,

$$\Theta(\xi) = 1 + \frac{(\gamma - 1)\, M_o^2}{6} \left\{ \arctan\left(\xi^2\right) - \frac{\xi^2}{1+\xi^4} - \frac{\pi}{2} \right\} \tag{19}$$

Differentiating the equation of state (13) with $\xi$ we have:

$$\frac{d\Pi}{d\xi} = \frac{1}{\gamma M_o^2} \left\{ \Theta \frac{d\beta}{d\xi} + \beta \frac{d\Theta}{d\xi} \right\} \tag{20}$$

or

$$\frac{d}{d\xi} ln(\beta\, \Theta) = \gamma\, M_o^2 \frac{V^2}{\xi \Theta}$$

Integration of the above equation and application of the boundary condition for the density when $\xi \to \infty$, yields,

$$\beta = \frac{c_1}{\Theta} exp\left( \gamma M_o^2 \int_0^{\xi} \frac{V^2}{\xi \Theta} d\xi \right) \tag{21}$$

where

$$c_1 = \frac{1}{exp\left( \gamma M_o^2 \lim_{L \to \infty} \int_0^{L} \frac{V^2}{\xi \Theta} d\xi \right)}$$

The pressure is then determined using Eq. (20). The above integrals are easily evaluated by any of the standard numerical methods say Rombergs, or better the application of software like *mathematica*, *maple*, or *matlab*.

The exact solution given in Eq. (19) can then be used to validate the numerical integration. The results for vortex Mach numbers of 0.8, 0.6, and 0.4 are shown in Fig. 2. It is clear from the figure that the numerically obtained $\Theta$ results compare well with the exact values. As a matter of fact the two sets of values are exactly the same up to the sixth decimal (for $L = 10,000$).

Next the sensitivity of the results to the value of the $Pr$ number was examined. In one atmosphere and 300 °K, the values of Prandtl number for most of the common gases are about 0.7, see Table 1. A 7.4 % difference in $Pr$ (if one takes $Pr$ to be 2/3 for Nitrogen instead of the actual 0.716) produces maximum errors which are less than 0.2% and 0.05 % in temperature distributions for $M_o$ = 0.8, and 0.4 respectively. The temperature for $Pr$ = 0.716 was obtained solving Eq. (18) using numerical integration. Therefore, in this investigation we will use the simpler exact expression for $\Theta$ to study vortices that have $Pr$ numbers in the neighborhood of 0.7 without suffering a substantial physical loss.

Table 1. Prandtl number of different gases at one atmosphere and 300 °K

| Gas | Pr |
|---|---|
| Air | 0.707 |
| Helium | 0.680 |
| Hydrogen | 0.701 |
| Nitrogen | 0.716 |
| Oxygen | 0.711 |

The analysis assumes a perfect gas, which implies that all the material properties are constant. In reality however properties such as $c_p$, $k$, and $\mu$ do depend on the temperature. In order to be pragmatic, the applicability of the solution should be limited to small temperature variations say around 300 K.

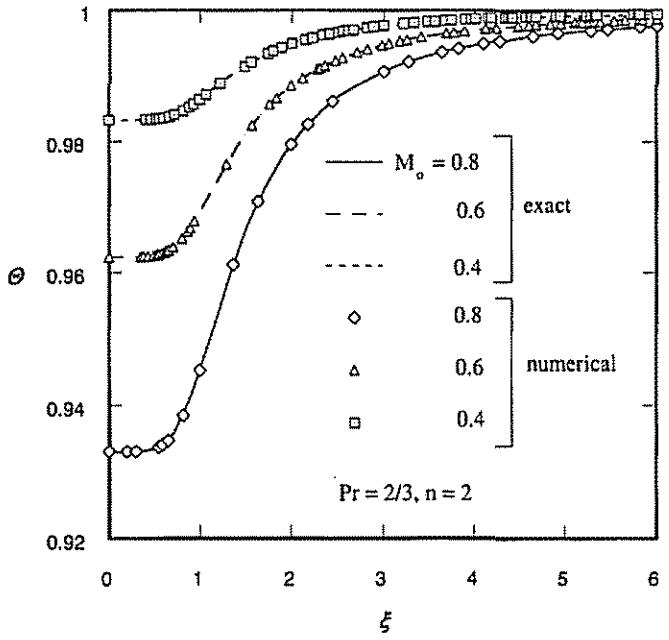


Figure 2. Exact and approximate temperature distribution for different Mach numbers.

Solutions for ideal conditions such as the isentropic flow are often useful because they provide a sense of direction and sometimes furnish acceptable approximations to the real problem. Under the constant entropy flow hypothesis, all the processes must be

reversible and adiabatic which requires the flow to be inviscid and the velocity components in the $r$ and $z$ directions must be zero. Then, the equations of continuity, $\zeta$-momentun, and energy will automatically be satisfied. The $\xi$-momentum is given by Eq. 10. The $\theta$-momentum, Eq. 4, simplifies into:

$$\beta u \left( \frac{\partial V}{\partial \xi} + \frac{V}{\xi} \right) = 0 \tag{22}$$

Since $u = 0$, the above equation will also be satisfied automatically regardless of the tangential velocity form.

For an isentropic flow,

$$\Pi = \frac{\beta^{\gamma}}{\gamma M_o^2}$$

Based on the above relation along with the $\xi$-momentum and state equations, taking the tangential velocity to be that of an $n = 2$ vortex, the exact solutions for the pressure, density, and temperature are:

$$\Pi = \frac{1}{\gamma M_o^2} \left\{ 1 - \frac{\gamma - 1}{2} M_o{}^2 \left( \frac{\pi}{2} - arc\,tg\, \xi^2 \right) \right\}^{\frac{\gamma}{\gamma - 1}} \tag{23}$$

$$\beta = \left\{ 1 - \frac{\gamma - 1}{2} M_o{}^2 \left( \frac{\pi}{2} - arc\,tg\, \xi^2 \right) \right\}^{\frac{1}{\gamma - 1}} \tag{24}$$

and

$$\Theta = 1 - \frac{\gamma - 1}{2} M_o{}^2 \left( \frac{\pi}{2} - arc\,tg\, \xi^2 \right) \tag{25}$$

The present density expression is equivalent to the one derived by Bagai and Leishman[7]. Note in passing that the $n = 1$ member of the $n$ - family can also provide an explicit isentropic solution[7].

Consider now the corresponding optical problem in Cartesian geometry shown schematically in Fig. 3. The analysis to follow, where the gas density $\rho$ in the test section is assumed to change only in the $y$-direction, was adapted mainly from Goldstein[12].

If the initial light intensity is $E_\infty$ then the intensity on the image plane $E$ will be,

$$E = \frac{1}{\lim_{\delta y \to 0} \frac{\delta y_{im\,pl}}{\delta y}} E_\infty \quad \text{where} \quad \delta y_{im\,pl} = \delta y + l\,\delta\alpha$$

or

$$\Sigma = \frac{E}{E_\infty} = \frac{1}{\left| 1 + l \frac{\partial \alpha}{\partial y} \right|} \tag{26}$$

It is possible in the problem under consideration for the rays to cross over. In order to make sure that $\Sigma$ remains always positive, the absolute sign has been incorporated into the above equation.

Since the angle $\alpha$ is given by[7]

$$\alpha = \frac{1}{\eta_\infty} \int_{l_1}^{l_2} \frac{\check{Z}\eta}{\check{Z}y}\, dz = \frac{l_2 - l_1}{\eta_\infty} \frac{\check{Z}\eta}{\check{Z}y} \tag{27}$$

then

$$\Sigma = \frac{1}{\left| 1 + \frac{l(l_2 - l_1)}{\eta_\infty} \frac{\partial^2 \eta}{\partial y^2} \right|} \tag{28}$$

where $\eta$ is the refraction index and $\eta_\infty$ is its value far from the vortex center ( $y \to \infty$ ).

The index of refraction is defined as the ratio of the speed of light in vacuum to the speed of light in the medium under consideration. Because in dilute gases the speed is only slightly less than in vacuum[1] the simplified version of the Lorenz-Lorentz equation, known as the Gladstone-Dale relation, is:

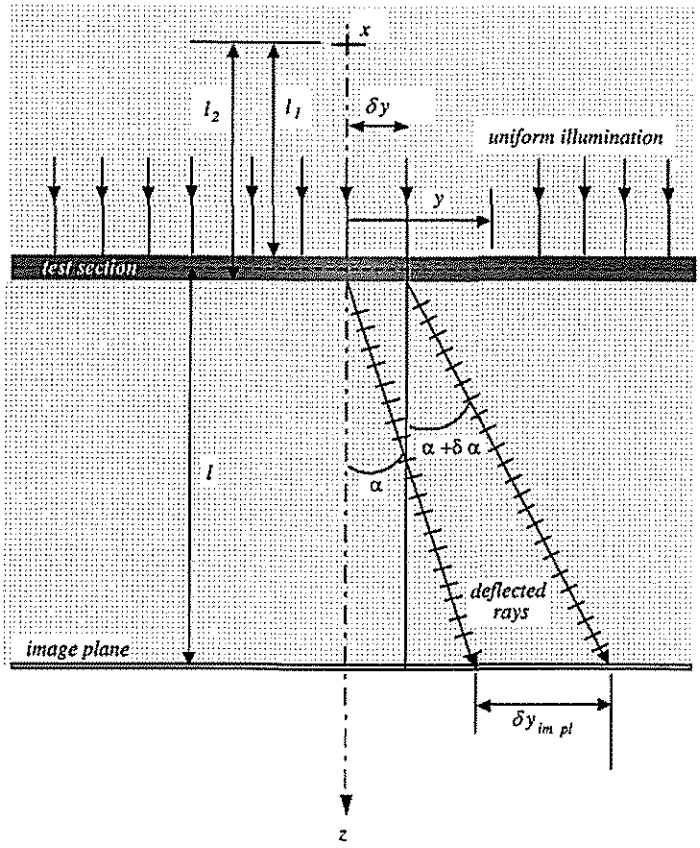


Figure 3. Schematic of the optical side of the problem.

$$\frac{\eta - 1}{\rho} = const = C$$

The last is found to approximate reasonably well real gases[12]. Using the last formula, Eq. (28) becomes

$$\Sigma = \frac{1}{\left| 1 + \frac{l(l_2 - l_1) C}{\eta_\infty} \frac{\partial^2 \rho}{\partial y^2} \right|}$$

The above expression in polar geometry, assuming axisymmetric density variation, is

$$\Sigma = \frac{1}{\left| 1 + \frac{l(l_2 - l_1) C}{n_\infty} \left\{ \frac{1}{r} \frac{\partial \rho}{\partial r} + \frac{\partial^2 \rho}{\partial r^2} \right\} \right|} \tag{29}$$

or in dimensionless form

$$\Sigma = \frac{1}{\left| 1 + \Lambda \, \Delta \right|} \quad \text{where} \quad \Lambda = \frac{\lambda(\lambda_2 - \lambda_1)\sigma}{n_\infty}, \quad \Delta = \frac{1}{\xi} \frac{\partial \beta}{\partial \xi} + \frac{\partial^2 \beta}{\partial \xi^2}, \tag{30}$$

$$\lambda = \frac{l}{r_c}, \lambda_1 = \frac{l_1}{r_c}, \lambda_2 = \frac{l_2}{r_c}, \text{ and } \sigma = \rho_\infty C$$

For isentropic flow conditions

$$\Delta = \frac{M_o{}^2}{\left(1 + \xi^4\right)^2} \left\{ 2\left(1 - \xi^4\right)\Theta + (2 - \gamma) M_o{}^2 \xi^2 \right\} \Theta^{\frac{3-2\gamma}{\gamma-1}} \tag{31}$$

For a more pragmatic analysis the expression of $\beta$ given by Eq. (21) must be used to evaluate $\Delta$ in Eq. (30).

## 3. Results and Discussion

Supplementary information on the physics of the compressible $n = 2$ vortex model can be found elsewhere[11]. Here only a brief description of the flow properties that is pertinent to the present analysis will be given.

The pressure, density, and temperature profiles for a Mach number equal to 0.8 are given in Fig. 4. It is evident that all three properties decrease along the flow direction attaining minimum values at the vortex center. Under the isentropic flow constraint, all curves have similar shape as the more general case. Besides the static pressure where the difference between the present and the past isentropic calculations is small, the homentropic hypothesis underestimates the temperature and overestimates the density inside the core. Therefore, one expects the optics to be affected by this difference. A similar behavior of these properties is also observed for Mach numbers of 0.6 and 0.4 [11].

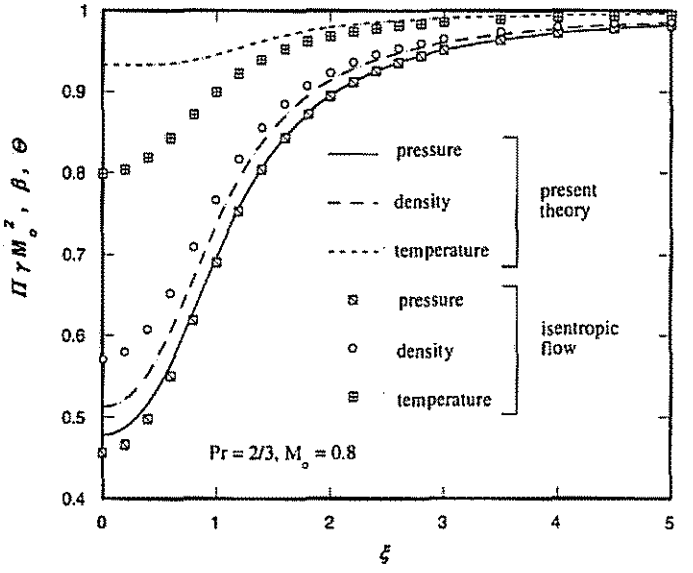


Figure 4. The static pressure, density, and temperature under the general and isentropic flow assumptions.

Given an illuminated vortex, $l_1$, $l_2$, $\rho_\infty$, $r_c$, and $\eta_\infty$ are constants. Consequently, varying $\Lambda$ is the equivalent of changing the focusing distance $l$. Typical light intensity profiles on the image plane, for a relatively shallow focusing (small $l$) and for three different Mach numbers are shown in Fig. 5. The intensity inside the core is always lower than the background illumination value marking the emergence of a dark disk in the image plane; see Fig. 6 (a).

Since the $\Sigma$ values are larger than one, within a circular band near the dimmer center, the dark nucleus is surrounded by a bright halo. At large radii the luminous intensity is seen to approach asymptotically its background value. The latter is very similar to the observed shadowgraph of Sterling et al.[3] and Bagai and Leishman[7]. As the vortex Mach number increases, the dark disk of the center becomes darker and the surrounding halo becomes more luminous.

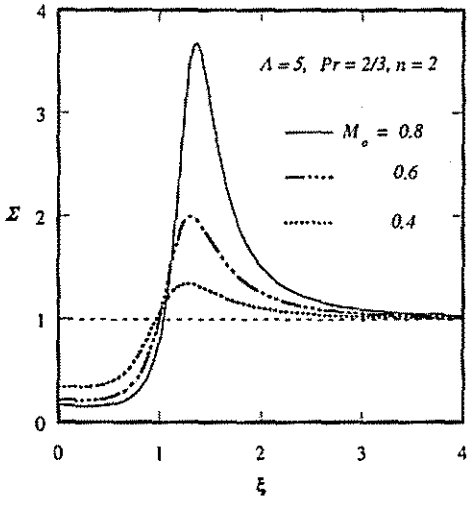


Figure 5. Light intensity profiles on the image plane for different Mach numbers.

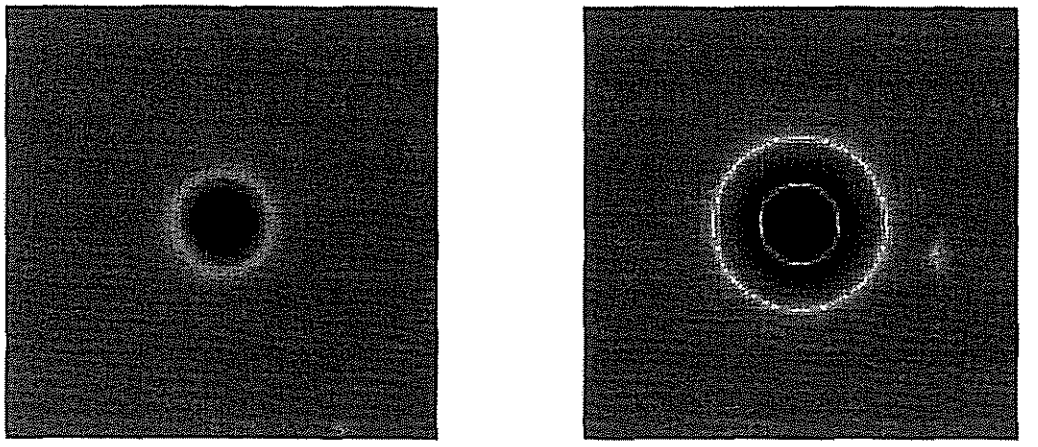

(a) (b)

Figure 6. Computed vortex shadowgraphs (a) $\Lambda = 5$ and (b) $\Lambda = 25$. In both cases $Pr = 2/3$ and $M_o = 0.8$.

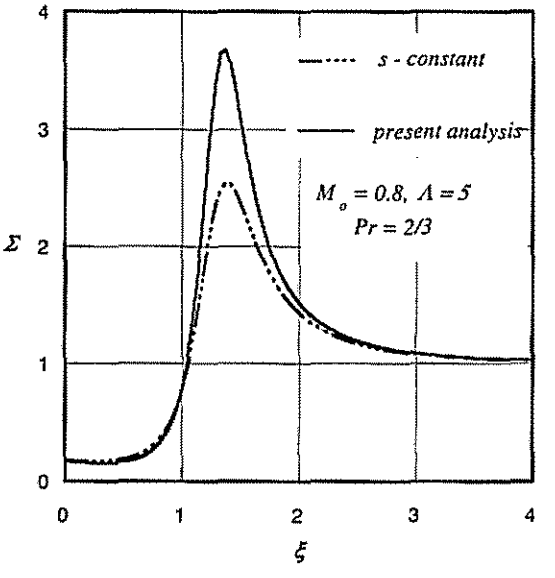


Figure 7. Intensity profiles under isentropic and the less restrictive present conditions.

The present results are compared with the isentropic formulation of Bagai and Leishman[7] in Fig. 7. Although the qualitative nature of the phenomenon was retained by the homentropic hypothesis, the improved analysis yielded a slightly dimmer vortex center and a considerably brighter corona. In agreement with the conclusions of the previously cited reference, the darkest area in the image plane is not at the vortex center but is rather displaced to the positive radial direction residing always within the core.

Depending on the value of $\Lambda$, various refracted patterns on the image plane can be obtained. Focusing on a larger depth, the theory suggests the formation of two caustic rings; see Figs. 8 and 6 (b), which is similar with the visualization experiments of Berry and Hajanal[2]. The transition from one caustic to two is relatively gradual. As $\Lambda$ increases the apex of the bright ring develops a dip, which propagates downwards creating an annulus of reduced brightness and the two caustics start to emerge. At a certain interval of $\Lambda$ values the two caustics begin to move apart. Then a second characteristic value of $\Lambda$ is reached, where the two caustics are in full view containing dark annuli (luminous intensity less than the background). A further increment of $\Lambda$ causes the dim annuli to become darker.

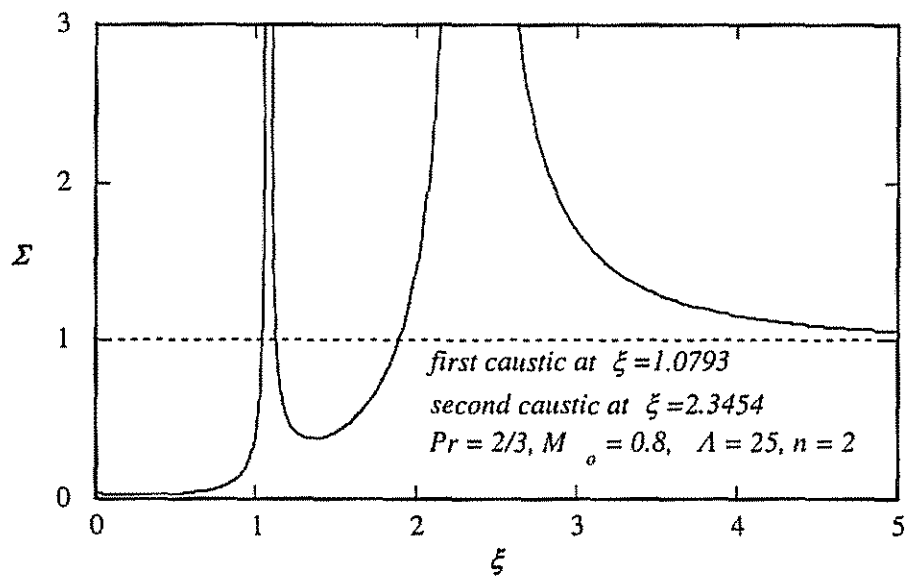


Figure 8. Light intensity distributions for deep focusing.

Swanson and Light[6] presented experimental shadowgraphs of rotor tip vortices with what appeared to be an odd set of alternating dark and bright circular bands. Based on the earlier work of Parthasarthy et al.[5], Bagai and Leishman[7] rightfully suggested that

perhaps this peculiar manifestation might be attributable to a very unusual density profile, remarking that the reasons behind this unusual behavior remain to be understood. The present analysis indicates that such a shadow formation may appear at larger $l$ (or $\Lambda$) values. The latter optical manifestation is also analogous to the observed Berry and Hajanal[1] light pattern with two caustics.

The dark disk boundary ($r_d$) was found to depend strongly on the vortex Mach number but insignificantly on $\Lambda$, see Fig. 9 (a) and (b). The latter border does not mark the core radius. For $n = 2$ the isentropic formulation $r_d$ is always larger than the core; while for the present theory it is smaller for Mach numbers less than 0.6 and larger when $M_o$ is greater than 0.6. Therefore, taking $r_d$ to represent the viscous core[5], errors ranging from ~ 2% ($M_o = 0.4$) to ~ 5% ($M_o = 0.8$) will be made. The present analysis suggests also that the last two parameters ($r_d$ and $r_c$) will coincide only for $M_o = 0.6$.

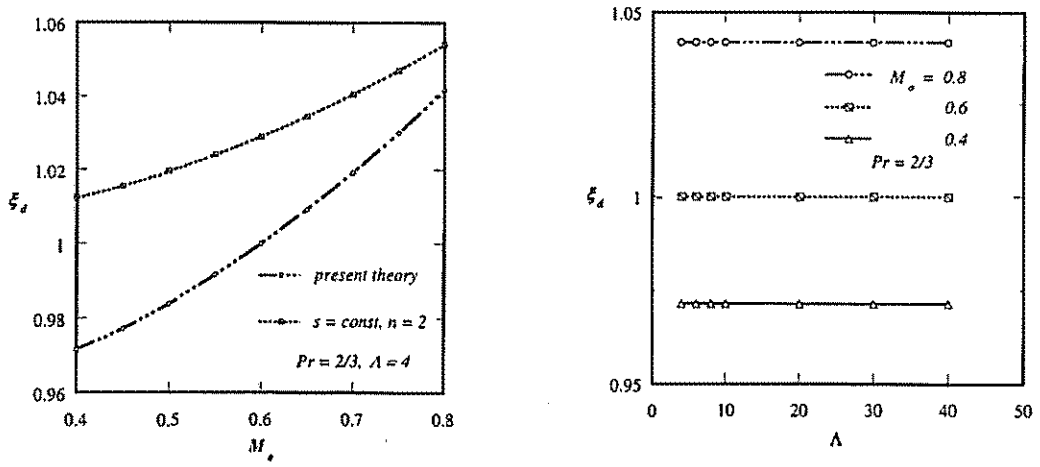


(a) (b)

Figure 9. Variation of the dark disk boundary as a function of (a) the vortex Mach number and (b) the image length $\Lambda$.

The presently developed methodology could now be used to advance the previous experimental descriptions[5-7,9] and provide a method for finer future correlations for the optics of compressible vortices.

## 4. Conclusions

The paper dealt with the refracted shadows generated by compressible vortices. A more realistic picture of the optical phenomenon precipitated when the flow instead of being isentropic is permitted to conduct and convect heat, and dissipate mechanical energy. Although the constant entropy hypothesis was shown to preserve the qualitative nature of the optics it fell short in portraying the quantitative side. It was clearly shown that the dark disk boundary does not mark the vortex core radius assumed in previous investigations. The more pragmatic analysis rendered the center of the vortex slightly darker and the halo considerably brighter than the earlier isentropic flow estimates. Furthermore, it identified an alternate explanation for the cause of the alternating dark and bright circular bands, evident in some of the past shadowgraphs of helicopter rotor tip vortices The present methodology can now be used to improve the experimental description of compressible vortices via the optical method of shadow.

REFERENCES


[1] Liepman, H. W. and Roshko, A. "Elements of Gas Dynamics". John Wiley & Sons, Inc., New York, 1957.

[2] Berry, M. V. and Hajanal, J. V. "The Shadows of Floating Objects and Dissipating Vortices". *Optica Acta*, **30** (1), 1983, pp. 23-40.

[3] Sterling, M. H., Gorman, M., Wildmann, P. J., Coffman, S. C., Strozier, J. and Kiehn, R. M. "Why are these Disks Dark? The Optics of Rankine Vortices". *Phys. Fluids*, 30 (11), November 1987, pp. 3624-3626.

[4] Landau, L. D. and Lifshitz, E. M. "Fluid Mechanics". Second Edition, Pergamon Press, 1987, Oxford.

[5] Parthasarthy, S. P., Cho, Y. I., and Back, L. H. 1985 "Wide-Filed Shadowgraphy of Tip Vortices from a Helicopter Rotor". *AIAA J*, **25** (1), January 1987, pp. 64-70.

[6] Swanson, A. A, and Light, J. S. "Shadowgraph Flow Visualization of Tiltrotor and Rotor/Wing Waves". Proceedings of the 48th Annual Forum of the American Helicopter Society, Washington, DC, June 3-5, 1992.

[7] Bagai, A. and Leishman, G. J. "Flow Visualization of Compressible Vortex Structures using Density Gradient Technique", *Exp. Fluids*, Vol. 15, 1993, pp. 431 - 442.

[8] Van Dyke, M. "An Album of Fluid Motion". The Parabolic Press, 1982, Stanford, California.

[9] Norman, T. R. and Light, J. S. "Rotor Tip Vortex Geometry Measurements Using the Wide-Field Shadowgraph Technique". *Journal of the American Helicopter Society*, **32** (2), 1987, pp. 40-50.

[10] Vatistas, G. H. "New Model for Intense Self-Similar Vortices". *AIAA, JPP*, **14** (4), 1998, pp. 462-469.

[11] Vatistas, G. H. and Aboelkassem, Y. The Compressible $n = 2$ Vortex". Under consideration for publication, in the *AIAA J* (TN), (July 2005)
[12] Goldstein, R. J. "Fluid Mechanics Meassurements". Hemisphere Publishing Co., New York, 1983.
[13] Vatistas, G. H. and Aboelkassem, Y. "Time Decay of $n$ Family of Vortices". *AIAA, J*, **43** (6), June 2005, pp. 1389-1391.
[14] Burgers, J.M., "A Mathematical Model Illustrating the Theory of Turbulence". *Adv. in App. Mech.*, Vol. 1, 1948, pp. 171-199.
[15] Sullivan, R. D. A "Two-Cell Vortex Solution of the Navier-Stokes Equations". *Journal of the Aerospace Sciences*, **26**, No. 11, 1959, pp. 767-768.
[16] Kalhoran, I.,M., & Smart, M. K. "Aspects of Shock Wave-Induced Vortex Breakdown". *Progress in Aerospace Sciences*. **36**, 2000, pp. 63-95.
[17] Cattafesta, L. N. and Settles, G. S. "Experiments on Shock/Vortex Interaction". AIAA Paper 92-0315, 1992.
[18] Mandella, M. J. "Experimental and Analytical Studies of Compressible Vortices". PhD thesis, Dept. of Applied Physics, Stanford University, 1987.